

Functional-Friction Networks: New Insights on the Laboratory Earthquakes

H.O. GHAFFARI,^{1(a)} B.D. THOMPSON² and R.P. YOUNG¹

(a)E-mail: h.o.ghaffari@gmail.com

¹ Department of Civil Engineering and Lassonde Institute, University of Toronto, Toronto, 170 College Street, M5S3E3, ON, Canada

² Mine Design Engineering, Kingston, Canada

Abstract –Using a recently proposed functional friction network approach constructed on the recorded acoustic emission waveforms from precursor events, we propose that the kinetic energy of the ruptures can be extended in terms of network's motifs. We show that the transition from the regular to slow ruptures can have a third production from the critical rupture class, comparable with the direct observations of this phenomena in the transparent samples. Furthermore, we show sub-micro accelerating and decelerating of the interface due to the short-term evolution of rupture tip, which lead to the introducing novel phase spaces for acoustic emissions.

Introduction- The 2011 Tohoku-Oki earthquake ($M_w=9.0$) showed how a slow slip phenomena can lead to the destructive ruptures, with emerging successive rupture transitions from slow to sub-Rayleigh and to super-shear ruptures [1-3]. Such a dramatic transition from creep fronts or slow slip events (SSE) to fast and sometimes critical ruptures has been reported in laboratory earthquakes: slow phase to fast, slow to critical phase and regular (fast) ruptures to super shears have been examined in transparent and rock materials [4-8]. The well-theoretical studied rupture transition is ruptures from regular rupture to super shear in which a characteristic length of the initial rupture in addition to a critical value (i.e., seismic ratio) regarding to friction force must be satisfied to emerge a “jump” in rupture velocity [9-11]. Recently a few numerical models have studied the evolution of creeping faults or SSE into critical earthquakes [12-14]. The models use the coupling of friction laws with heat and pore pressure, while the assumption of releasing huge thermal energy is a vital part of the equations. Obviously, in these models the weakening of the frictional –rock interface (i.e., fault) is due to rapid shear heating of pore fluids and does not accord with the experimental observations where simple mechanical loadings can guide such dramatic phase transitions. As well as the mentioned developments, recent precise laboratory measurements have presented new insight in to sub-micron events [6, 15]. Among them, finding fairly universal trends of appropriate parameter spaces was much of interest [6].

To support the aforementioned ideas, very recently, the authors used complex network techniques to extract “hidden” information from recorded waveforms as well as reconstructed or recorded images through simple friction-tests to complicate the loading (boundary) conditions of glassy and rock samples [7]. We showed that

functional networks constructed over little sub-micron events (“precursor or fore shocks” laboratory earthquakes) can unravel the possible regime of the rupture while the changes of dynamic phases of network parameters are correlated with weak to very powerful events [7]. In addition to this, using our network algorithms, we proved the general asymmetric nature of acoustic emissions as the class of crackling noise systems. In this study, using the proposed functional friction networks, we explore the transition regimes of ruptures in Westerly granite- frictional interfaces. To this aim, we use several network parameter spaces while the energy of the obtained networks (and then acoustic pulses) is analyzed using modularity profiles. Interestingly, we find that our phenomenological formulation based on the functional friction networks presents an unprecedented solution to dramatic rupture transitions in laboratory scale. As well, building on the evolutionary phases of modularity’s indexes, we present a new way to estimate fracture energy where a glass transition period is matched with a rapid evolutionary phase of modules’ fast-growth. Our results from the trends of the fracture energy in different regimes of ruptures confirmed the recent theoretical and numerical studies regarding the physics of fracture energy. Furthermore, a slip-weakening model, constructed upon the frictional resistivity of the interfaces is proposed where the resistivity-slip rate phase space is related to our networks’ attributes. To complete our analysis, we developed a mean-field approach on the power law distribution of centrality, which lead to a phase diagram with a fit-get-rich-phase while we change the control parameter of the model. We show how the model can reach a gel-like or condensed state and interpret the “gel-like” functional friction networks as the “super-lubricity” regime.

Reviews of experiments -The detailed experimental results have been reported in [16-17]. Our main data set includes the recorded discrete and continuous waveforms (i.e., acoustic emissions-AEs) using 16 piezoelectric transducers from a saw-cut sample of Westerly granite (LabEQ1), under triaxial loading [16-17]. The saw cut was at a 60 degree angle and polished with silicon carbide 220 grit. Each triggered event had the duration of 204.8 μ s (recorded at 5 MHz), while the three main stick-slip events occurred. The experiment was servo-controlled using an axial strain rate of $5 \times 10^{-6} s^{-1}$ ($\sim 10 \mu m / s$ as the loading rate). The confining stress was maintained at 150 MPa for three reported main stick-slip events, producing 109 located- rupture fronts events. The second data set (LabEQ2) are the results of the two main cycles of loading –unloading (stick-slip) of Westerly granite on a preexisting natural fault by loading at constant confining pressure. A natural rough fault was created using a triaxial loading system at the constant confining pressure of 50 MPa and with acoustic emission feedback control.

Functional-friction networks– The application of recurrence networks as new tools to analyze time-series has been the subject of the numerous research areas during last decay [18]. An important advantage of recurrence networks is that their performance and outputs are very good, while the time series are significantly short [19, 20]. The main issue in recurrence networks is the selection of the best truncation level of a metric to

form a “functional” network (i.e., indirect construction of graphs). To this class of recurrence networks, several methods have been suggested. Among them, one can consider the density of links, betweenness centrality, motifs’ density and percolation based methods [21-26]. A recent proposed recurrence networks’ meta-time series considers the power of the multi-observation of an event or series of events through different observatories [20, 27]. We recently employed a similar meta-time series analysis on the quasi-static evolution of apertures and real-time contact areas [28-29]. In [7], we showed that the nature of piezoelectric signals can be quantified through this new tool, resembling slip patterns on a sub-micron scale. Here we review the previously introduced algorithm. The first step is the normalization of waveforms in each station and then the division of N - recorded time series with the length of T into m segments. The j th segment from i th time series ($1 \leq i \leq N$) denoted by $x^{i,j}(t)$ is compared with $x^{k,j}(t)$ to create an edge among the aforementioned segments. If the j th segment of the i th and k th time series are “close” enough to each other, we set $a_{ik}(j) = 1$ otherwise $a_{ik}(j) = 0$ in which $a_{ik}(j)$ is the component of the connectivity matrix. We use a “closeness” metric: $d(x^{i,j}(t), x^{k,j}(t)) = \sum_t \|x^{i,j}(t) - x^{k,j}(t)\|$. To select a threshold level, we use betweenness centrality (B.C). The details of the method have been explained in [28-29], and it has been proven that using this method quantitatively is equal to using edge density. The advantage of the method is insensitivity for a range of the threshold level. To precisely analyze a time series with the aforementioned methods, we set $m=1$ (equal to each recorded point). This essentiality considers the high temporal- resolution of the systems’ evolution, smoothing the raw signals with 20-60times window (for Lab.EQ1& 2 is equal to 1-3 μs). To decrease the sensitivity of the networks and knowing that recurrence networks—generally- reveal a good performance in a small number of nodes, we increased the size of the adjacency matrix with the simple interpolation of d using cubic spline interpolation. Further analysis shows that the method is nearly insensitive for $N > 15$. The increasing of the number of nodes generally did not change the presented results and merely increased the quality of visualization of the results. Then for the acoustic-friction networks, the numbers of nodes are 50 and the number of nodes is kept as the constant value. We use some main characteristics of networks which we will use as the basis for our modeling. Each node is characterized by its degree k_i and the betweenness centrality (B.C) as the measure of “load” in networks [30]:

$$B.C_i = \frac{1}{(N-1)(N-2)} \sum_{h \neq j, h \neq i, j \neq i}^N \frac{\rho_{hj}^{(i)}}{\rho_{hj}} \quad (1)$$

in which ρ_{hj} is the number of the shortest path between h and j , and $\rho_{hj}^{(i)}$ is the number of the shortest path between h and j that passes i . The main celebrated diagnostic in our networks is modularity index or *Q-profiles*. The networks’ modularity characteristic is addressed as the quantity of densely connected nodes relative to a

null model (random model). In particular, based on the role of a node in the network modules or communities, each node is assigned to its within-module degree (Z) and its participation coefficient (P). High values of Z indicate how well-connected a node is to other nodes in the same module, and P is a measure of the well-distribution of the node's links among different modules [30-33]. The modularity Q (i.e., objective function which we are looking to maximize that) is defined as [32]:

$$Q = \sum_{s=1}^{N_M} \left[\frac{l_s}{L} - \left(\frac{d_s}{2L} \right)^2 \right], \quad (2)$$

in which N_M is the number of modules (clusters) , $L = \frac{1}{2} \sum_i^N k_i$ is the number of links in module and

$d_s = \sum_i k_i^s$ (the sum of nodes degrees in module s). Using an optimization algorithm, the cluster with maxi-

mum modularity (Q) is detected. The number of triangles surrounding a node, denoted by T_i , is used to define the clustering coefficient; an index as the normalized value of triangles (or the simplest loops or 3-point motifs):

$$c_i = \frac{2T_i}{k_i(k_i - 1)}.$$

Network's Phase Spaces of AEs events – Accomplishing the aforementioned algorithm on acoustic-emission data set, we obtain a typical Q-profile for each single event (Fig.1a). This profile presents some basic ingredients of a single event as the result of breaking an asperity or generally a “node”. In the following, we show how this modularity index represents a generic dynamic of a single asperity failure, opening a new window into the laboratory earthquakes and material science. Inspecting many events from Lab.EQ1 and Lab.EQ2 revealed that the general evolutions of modules are universal, imprinting nearly constant characteristics of timescale per each evolutionary phase [7,15].The main evolutionary phases are as follows: phase 1 is the rapid dropping of modularity and reach to the minimum value of $Q(t)$, indicating the formation of a dense network. Considering that the laboratory earthquakes are in near-field, approaching the crack front, deformation or crushing the “node” or asperity is the possible explanation for this stage. The duration of this phase is 4-10 μs . Later ,we will use the inverse of the Q-profiles to amplify the first phase as the deformation phase and the resistivity function to picture the possible signature of frictional resistivity in sub-micron scales.

The immediate phase is the fast growth of modularity and increasing the number of modules as has been shown in Fig.1.a. As we have shown in [7], the rate of this rebounding phase is scaled with the maximum value of the modularity. The collapsed data set for this phase indicates a universal generic dynamic, which is confirmed by a constant value of the power law coefficient $\alpha \approx 1.5 \pm .3$ for both Lab.EQ1 and Lab.EQ2. The duration of this phase is 25-35 μs .The possible approach for this phase is the fast slip of the

interface which is arrested or damped at the end of the phase. Assuming a range of velocity for phase 2, 5-500 $\mu m/s$, we obtain the maximum displacement at the end of the phase 2 as $\sim 150\text{pm}-15\text{nm}$. The maximum displacement at the end of the phase 2 changes to 1-5 μm , if the frictional slip rate increases to 50-100 mm/s (the reported value for PMMA in [15]). This shows that the recorded precursor events encode a displacement magnitude at the range of pico to nano meter (and maximum micro), demonstrating possible nano-earthquakes in terms of the displacements of the interface. To be precise, the evolution of this phase is not quite linear and does have two main sub-classes: a linear and non-linear phase. This recent finding with having a nearly constant transition time scale implies a distinguished attribute of near-crack tip deformation. We will discuss this property somewhere else with more details.

The transition to the last evolutionary phase (phase IV) is accompanied by an unusual gradual decay of the communities (phase III). We will use a theory of glass transition to explain the emergence of this phase (see next section). The last phase generally is a decaying phase, indicating a slow-slip phase. The rate of this phase, RQ_4 , scales with the maximum recorded modularity as: $|RQ_4| \propto Q_{\max}^\lambda$ in which λ is a nearly constant for the regular events (supplementary document of [7]). Furthermore, a rough scaling between the rate of the first phase and the last phase was found [7]: $|RQ_{IV}| \propto |RQ_I|^{-\gamma}$ where γ is slightly larger for slow slip events. To get a spatio-temporal evolutionary picture of the recorded events, we use mean values of networks' diagnostics on all nodes and the monitored time-interval. Applying this idea on Lab.EQ1 and Lab.EQ2, we recognized several correlations between networks' attributes (Fig.1b,c and d). We will use the following scalar parameter spaces to develop phenomenological and mean-field models.

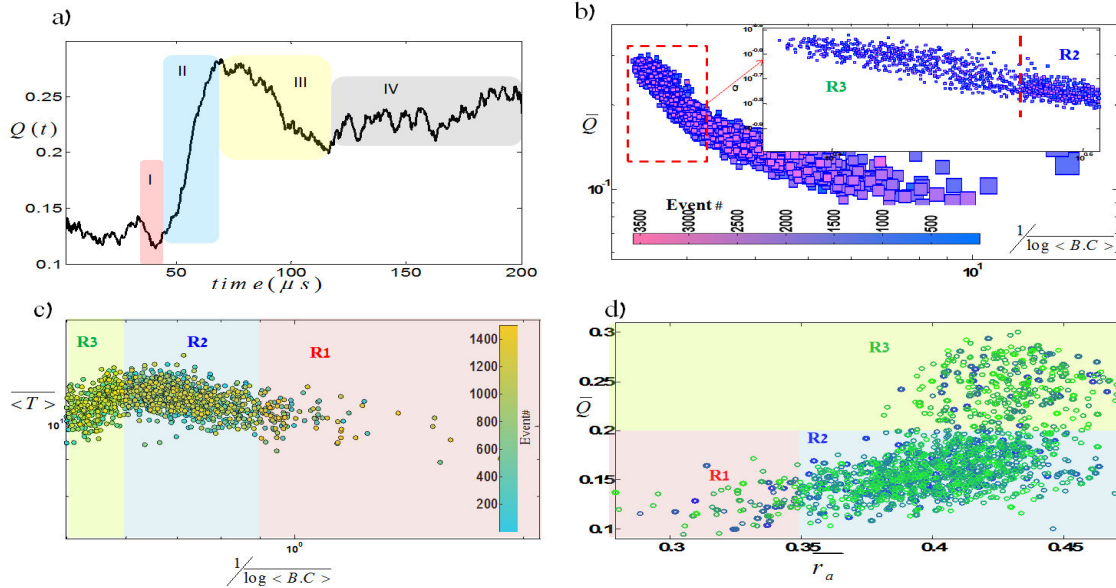


Figure 1|Evolution of rupture fronts in a rough fault. (a) Q-profile resulted from the mapping of acoustic waveforms from a regular event includes 4 main evolutionary phases [7].(b) ~3500 recorded acoustic emission events; the size of the squares corresponds to the maximum root mean square of the amplitudes of all piezoelectric sensors. The inset shows a crossover to R₂ class of events occurring after threshold level . (c) The scaling of $\frac{1}{\log \langle B.C \rangle}$ with the temporal average of triangles (3 points motif: $\langle T \rangle$) differentiates the three main clusters : $\langle T \rangle \propto \log \langle B.C \rangle^{-\chi}$. For any events, we have : $(\chi > 0, R_1)$ or $(\chi < 0, R_2)$ or $(\chi < 0, R_3)$. (d) Higher average assortativity scales with higher modularity value, with a separation in high modular fronts, characterizing slow slip ruptures.

In Fig.1b, we show one of the parameter spaces for Lab.Eq.2 : $\overline{\log \langle B.C \rangle}^{-1} - \bar{Q}$. For relatively high values of $\overline{\log \langle B.C \rangle}$, a remarkable cross-over from high-modularity to intermediate modularity is observed. For the saw –cut experiment, we found a unique separation of some events, providing a slow deformation (i.e.,R3 class) with respect to the duration of phase I and somehow a similarity to the phase IV [7]. A similar cross-over is observed in $\langle T \rangle - \overline{\log \langle B.C \rangle}^{-1}$ and $\bar{Q} - \bar{r}_a$ spaces. We recognize three main classes regarding this network-clustering: R1, R2 and R3. The R1 phase holds events with relatively high energy while events with the intermediate energy (“regular”) are allocated to the R2 class. The R3 class does have a longer evolutionary phase I and represents longer and weaker (on average) events, indicating a slow-lip phenomenon. Based on Fig.1b and c , we can write a power law function to cover the collapsed events : $\langle T \rangle \propto \overline{\log \langle B.C \rangle}^{-\chi}$ and $Q_{\max} \propto \Xi^{-\pi}$ in which $\Xi = \overline{\log \langle B.C \rangle}^{-1}$, π and χ are nearly constant exponents for each class. Obviously, transition from R3 to R2 class is equal to change of the sign of χ .

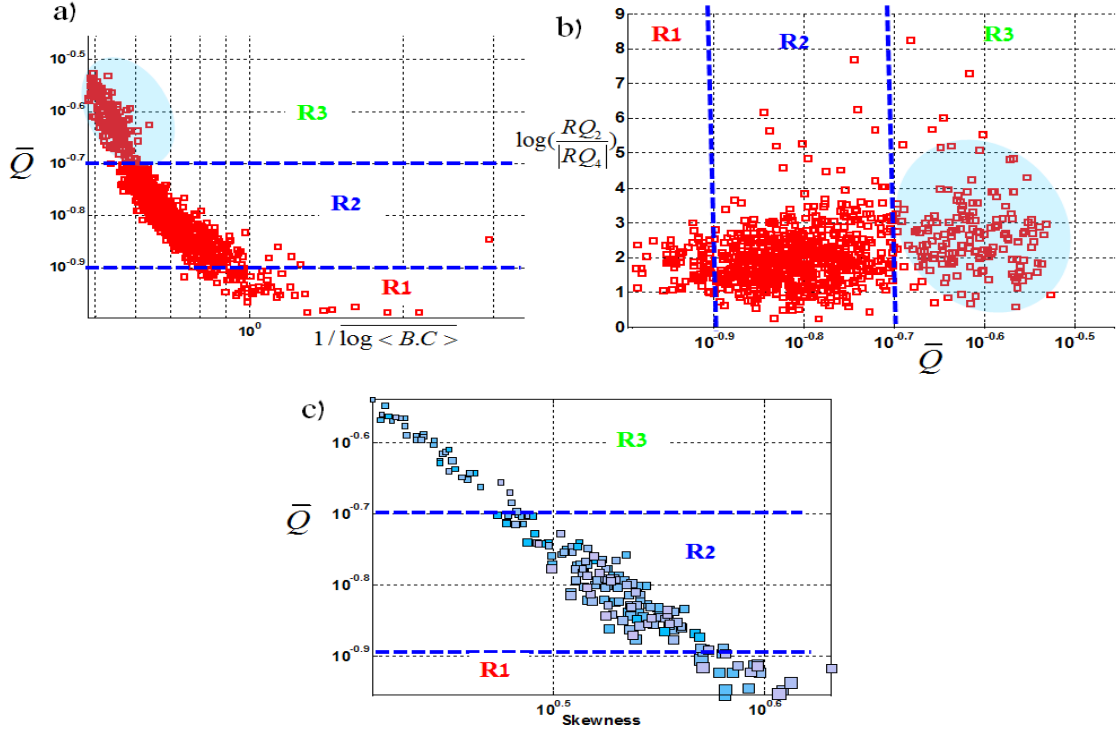


Figure 2| Asymmetric nature of Q-profiles. (a) $\log \langle B.C \rangle^{-1} - \bar{Q}$ space with three distinct classes. (b) the ratio of the rate of the second and last phases versus the mean modularity value ($\log\left(\frac{RQ_2}{RQ_4}\right) - \bar{Q}$). (c) The average skewness scales with \bar{Q} , indicating a smaller positive skewness of pulse shape hold events from R3 class (data from Lab.EQ2).

Furthermore, using networks' diagnostics, we can investigate the asymmetric nature of crackling noise pulses (including acoustic emissions). The average skewness of Q-profiles as the asymmetry measure can be quantified by [35]:

$$\Sigma = \frac{\frac{1}{T} \int_0^T Q(t)(t - \bar{t})^3 dt}{\left[\frac{1}{T} \int_0^T Q(t)(t - \bar{t})^2 dt \right]^{3/2}} \quad (3)$$

in which $\bar{t} = \frac{1}{T} \int_0^T Q(t) dt$ and $T = 204 \mu s$. In Fig.2.c, we have compared the skewness versus the mean modularity for the Lab.EQ2 events. An excellent collapsing of data in $\bar{Q} - \Sigma$ shows the evolution of the leftward asymmetric shape of the acoustic waveforms regarding the regime of ruptures. This is a universal feature of "crackling noise" systems which has been allocated to the nature of the dissipation energy (such as Eddy currents in Barkhausen noise (movement of magnetic domain wall) or threshold strengthening in moment rate

profiles in natural earthquakes [34-35]). From Fig2.b, we also infer that the $(\frac{RQ_2}{|RQ_4|})$ does have (on average) its minimum value for relatively high energy ruptures (or critical deformations), coinciding with the maximum asymmetry in Q-profiles. We conclude that more deviation from symmetry is the signature of ruptures with relatively high energy and critical ruptures while approaching a less asymmetric shape indicates ruptures with lower energy.

Next, to distinguish the role of the main deformation phase –phase I–we define a parameter of resistivity against motion, denoted by resistivity: $R \equiv \frac{1}{Q_{norm.}}$ where $Q_{norm.} = \frac{Q}{Q_0}$. In Fig.3b ,we have illustrated the

collapsing of events from Lab.EqQ1 in a normalized $(\dot{R})_I - R_{max.}$ space, indicating a nearly constant time scale for the first phase and for *most* of the events. This shows a generic dynamic with universal time characteristic controls the first phase as well as other evolutionary phases. Approaching the critical stage and failure phase and then fast-slip phase can be well-quantified by “ S_R -parameter”:

$$S_R = \frac{R_{max.} - R_0}{R_0 - R_{min.}}$$
 (Fig.3a-inset).

This parameter is similar to seismic S-factor: $S_s = \frac{\tau_p - \tau_0}{\tau_o - \tau_r}$ [9-11] which is defined over the variation of shear strength in a period of shear displacement. It has been widely discussed that the value of S_s could be used to determine the regime of rupture ; for instance it has been shown that below a critical value of $S_s < S_c$, a super-shear rupture may occur. In other words, by increasing S_s the probability of occurring “critical ruptures” is less and the regime of the rupture approaches to regular and under-regular ruptures. In Fig.3d, we have shown that S_R remarkably scales with the $Q_{max.}$ representing ruptures with smaller maximum modularity holds higher S_R , i.e., weaker and slower failures in sub-micron scales. Then, we can use “ S_R -parameter” in the possible classification of rupture fronts (Fig.3d). Interestingly, $R_{norm} - \dot{Q}$ shows a unique phase space resembling frictional resistance versus slip rates in centimeter and meter scales (Fig.3.b) [36].

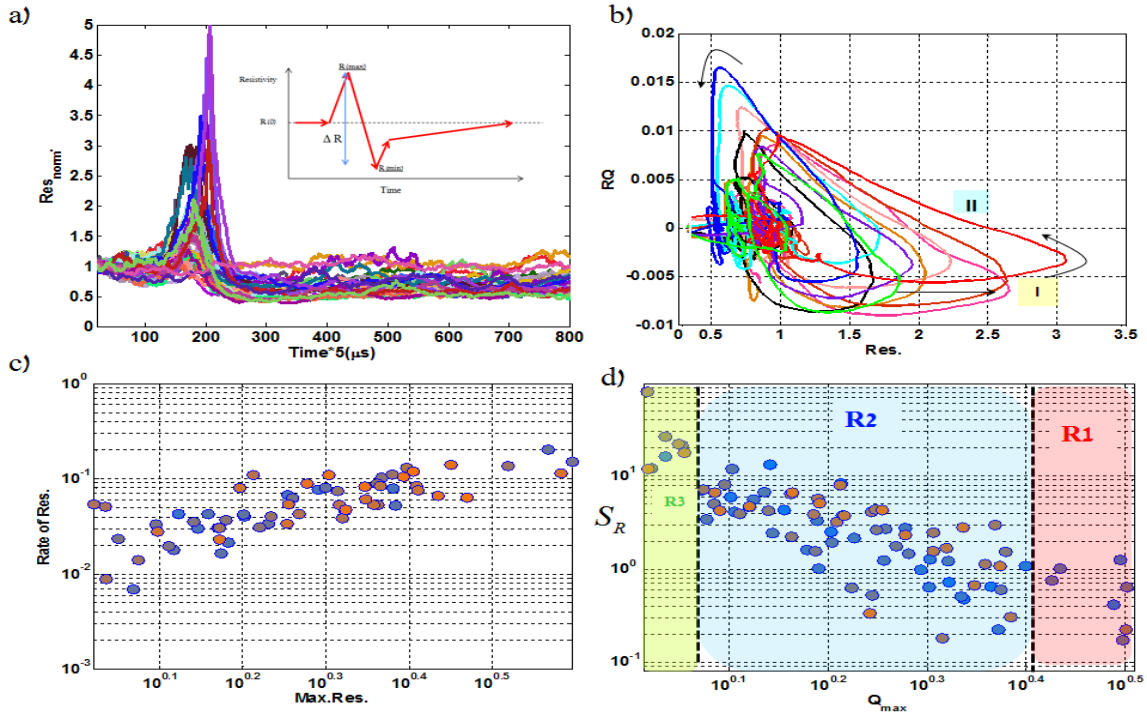


Figure 3| “Resistivity” and the onset of weakening. (a) The inverse of Q -profiles amplifies the evolution of the first phase. We assume the resistivity against the slip (or motion) is proportional to reciprocal of the Q values. We have shown ~ 30 arrested rupture fronts from Lab.EQ1 and their normalized resistivity parameter (Inset: a simplified form of the resistivity profiles parameters to define “ S ” parameter). (b) Phase space of events from Lab.EQ1 in $Res_{norm} - RQ$ plane (c) a nearly constant exponent (β) in $R_{Res} \propto Re_s^\beta$ represents a generic dynamic for the first evolutionary phase, indicating a nearly failure or deformation timescale. (d) Collapsing events in $S_R - Q_{max}^{norm}$ parameter space ($S_R = \frac{R_{max} - R_0}{R_0 - R_{min}}$), shows events with higher modularity show smaller S value while very small Q values hold a higher S values (events from Lab.EQ1).

To fit a model on the phase space (Fig.4), we use the fact that for “regular” ruptures the duration of the second phase (“fast-slip” or slip-weakening) phase) is nearly constant :

$$R = R_0 + A(R_p - R_0) \exp\left[\ln(0.03) \frac{t}{t_c}\right] \quad (4)$$

in which $R_0(RQ) = \exp\left(-\frac{RQ}{RQ_c}\right)$ and R_p is the maximum of resistivity . We found that $t_c \approx 70 \mu s$, $RQ_c = 0.004$, $A = 4$ and assigning $R_0 \equiv 1$ remarkably satisfies most of the recorded experimental results (Fig.4). Considering that t_c includes some dead time and the first phase duration, we conclude that $(t_c)_{real} \approx t_{II}$, *i.e.*, weakening time or fast slip duration .

It is worth mentioning that the presented equations are comparable with the results of high-velocity friction experiments, in which rotational shear experiments mimic long range of displacements of faults, sliding with variations of loading velocity [36].

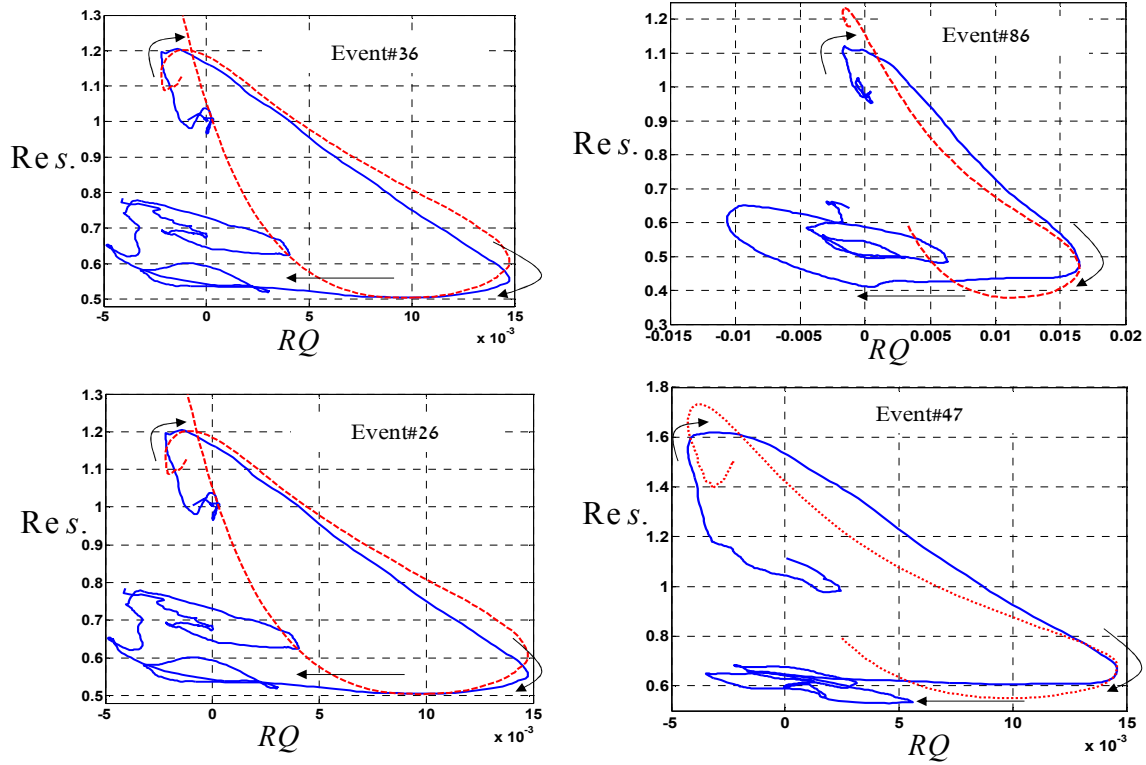


Figure 4 | Comparing the model with the experimental data. A comparison of phase space of precursor rupture fronts from smooth-rock interfaces in terms of rate of Q- profiles and resistivity between experimental data (blue) and friction modeled by presented equation (red-dashed line) .

Ruptures-Energy based on Modularity Rate – In this section, we will use some of the mentioned relations to establish a possible link with energy of ruptures. Moreover, we estimate fracture energy based on the revealed evolutionary phases durations and melting-glass transition approach. First of all, we show the energy of functional networks in terms of evolution of communities can be purely expressed in terms of motifs. To this end, we assign the kinematic energy of the rupture (system) to the rate of evolution of groups. In [37-39], an analysis of motifs of different networks proved that the functionality of networks was correlated with the motif’s profiles. We prove a weak form of this general approach where we consider the simplest closed motifs: triangles. If the energy of a system could be extended in terms of motifs, then we can expect that motif’s frequency is associated with the energy spectrum of the system. Considering $\overline{\langle T \rangle} \propto \overline{\log \langle B.C \rangle}^{-\chi}$, $|RQ_4| \propto Q_{\max}^{\lambda}$ and $Q_{\max} \propto \Xi^{-\pi}$ in which $\Xi = \overline{\log \langle B.C \rangle}^{-1}$, we reach to : $\overline{\langle T \rangle} \propto |RQ_4|^{\frac{-\chi}{\pi\lambda}}$.

we approximate the kinematic energy of the system as the energy of each evolutionary phase (shown in Fig.1a) in Q-profiles: $E_{system} \approx E_I + E_{II} + E_{III} + E_{IV}$. Also, we assume $E_{IV} \propto v_{IV}^2 \propto RQ_{IV}^2$ which leads to:

$E_{IV} \propto \langle \bar{T} \rangle^{\frac{-2\pi\lambda}{\chi}}$. This assumption is due to the similarity of Q-profiles to the recorded strains (normalized displacements) []. With ignoring the third phase, we estimate $E_I \propto RQ_I^2$ using $|RQ_{IV}| \propto |RQ_I|^{-\gamma}$ which reads

$E_{system} \propto \langle \bar{T} \rangle^{\frac{-2\pi\lambda}{\chi}} (1 + \langle \bar{T} \rangle^{\frac{(2\pi\lambda)(1+\gamma)}{\chi}} + E_{II})$. The last term is extended as follows: $E_{II} \propto RQ_2^2 \propto \langle \bar{T} \rangle^{\frac{-1}{2\chi\pi\alpha_2}}$ where α_2 is constant for *most* of the events. Eventually, we reach:

$$E_{system} \propto \langle \bar{T} \rangle^{\frac{-2\pi\lambda}{\chi}} (1 + \langle \bar{T} \rangle^{\frac{(2\pi\lambda)(1+\gamma)}{\chi}}) + \langle \bar{T} \rangle^{\frac{-1}{2\chi\pi\alpha_2}}, \quad (5)$$

in which $\{\pi, \lambda, \gamma, \alpha_2 > 0\}$ and it presents the kinematic energy of the pulse regarding Q-profiles. In other words, the energy of the waveforms is extended with motifs' frequency and some exponents.

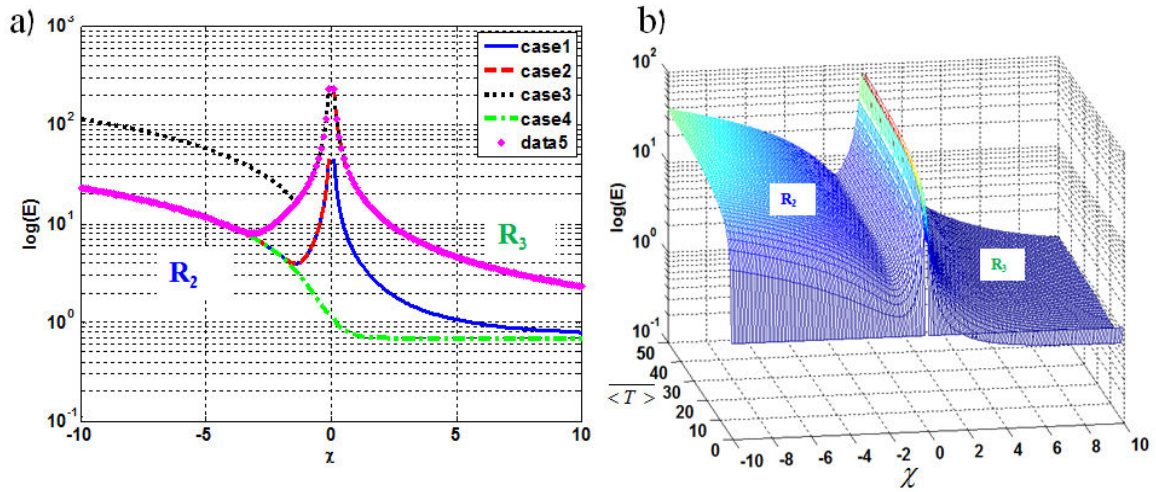


Figure 5|Study of rupture transition using energy of Q-profiles. (a) Variation of the kinematic energy with the exponent in $\langle \bar{T} \rangle \propto \overline{\log < B.C >^{-\chi}}$ -see the text-shows a singularity around $\chi = 0$ in which a transition from R_3 to R_2 occurs for $\langle \bar{T} \rangle = 10$. Case 1: $\pi = \lambda = \gamma = 1, \alpha = 2$; Case 2: $\pi = \lambda = 1, \gamma = 5, \alpha = 2$; Case 3: $\pi = 2, \lambda = \gamma = 1, \alpha = 2$; Case 4: $\pi = \gamma = 1, \lambda = 0.01, \alpha = 2$; Case 5: $\pi = \gamma = 1, \lambda = 5, \alpha = 2$. b) Kinematic energy varies with χ and $\langle \bar{T} \rangle$ for the first case.

When $\chi > 0$ (R_3 -regime-Fig.1c), increasing the loops pushes the system to a steady state with the minimum energy while for R_2 class, the increasing loops leads the system to a new energy level as the minimum upper bound of R_2 : $E_{system, \chi > 0} \propto \langle \bar{T} \rangle^{\frac{-2\pi\lambda}{\chi}} + \langle \bar{T} \rangle^{\frac{-1}{2\chi\pi\alpha_2}}$. We denote this upper bound, as the cross-over point from R_3 to R_2 (see Fig.5.a). In other words, we have shown the kinematic energy in the cross-over point (R_3 to R_2 and vice versa) changes dramatically, reassembling the first order transition. The obtained result is comparable to the direct-observation of transition from sub-Rayleigh to slow rupture mode [4-8]. This result also is com-

parable with our conclusions on PMMA-networks [29]. Furthermore, approaching $\chi \rightarrow 0$ from the right hand is different from the left hand and depends on the other scaling parameters, which will change. Remarkably, the transition from R_2 to R_3 class should have a unique signature: passing from $\chi \approx 0$.

At the same time approaching $\chi = 0$ does have another interpretation, comparable with reaching R_1 (or critical ruptures) class. Jumping or approaching the energy barrier as the singularity point of this phenomenological model can be interpreted as the generation of a high energy rupture, i.e., a signature of R_1 class. This interpretation is compatible with the observation of super-shear pulse (rupture) in PMMA – (reported in [1,2] –also see Fig.6). In fact, in [4], for the first time –experimentally- it has been shown that the transition from sub-Rayleigh ruptures to slow ruptures results in a third production rupture from super-shear rupture (Fig.6). This picture is very close to the 2011 Tohoku-Oki earthquake as it has been visualized in [] using high-resolution network of seismograms.

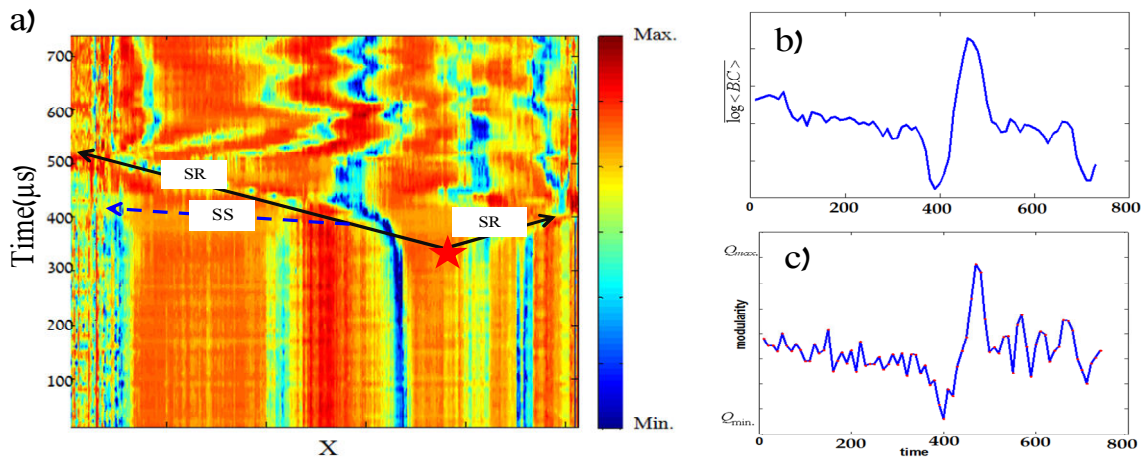


Figure 6] Transitions in Laboratory Ruptures. (a) z-score variation versus time over implementation of networks on real-time photo elastic of successive photos from Resin-Resin interface [8]. We have used a method introduced in [] to construct networks over raw images. The transition to sub-Rayleigh (SR) ruptures does have a production from high energy ruptures, super-shear ruptures (SS). This result previously has been confirmed by Fineberg’s group [4] ($X=14.5$ cm). (b,c) mean centrality and Q values for the shown rupture versus time in $\sim 700\mu s$ time-window. The data set courtesy of the original photo-elastic movie is from S.Nielson (INGV).

Interestingly, with assuming independency of scaling exponents to each other and approaching $\lambda \rightarrow 0$, R_3 class is vanished (Fig.5a). We conclude that λ, π, γ controls transitions to R_1 or R_3 , the sharpness of transition from R_2 to other classes and the evolution of R_3 class, respectively. Remarkably, the transition from R_2 to R_1 (or R_3) with approaching χ to $\chi = 0$ shows crossing from a minimum E , indicating a *jammed regime of the rupture*. The jammed state of the introduced-rupture’s phase diagram is important to understand because it can arrest the rupture as it propagates in energy landscape. The same behavior is observed when $\gamma \rightarrow 0$ while the transition from R_3 to R_1 is trapped in a jammed state (not shown). Moreover, using the results presented in [7], we connect $\overline{\langle T \rangle}$ to the remote stress (strain) field. To this end, we use

$\bar{Q} \propto \exp(-\kappa F_{axial})$ and $\bar{Q} \propto \Xi^{-\eta}$ which yields $\log \langle T \rangle \propto \frac{\chi \kappa}{\eta} F_{axial}$, in which $\kappa > 0$ and η are scaling exponents. F_{axial} represents external axial loading stress as the driving force (boundary condition). For the R_2 class ($\chi < 0$), decreasing $\langle T \rangle$ corresponds with the increasing external remote stress field while for $\chi > 0$, the trend of $\langle T \rangle$ is similar to F_{axial} . To get use of this scaling relation, we substitute $\log \langle T \rangle \propto \frac{\chi \kappa}{\eta} F_{axial}$ in to the energy term, yielding:

$$E_{system} \tilde{\propto} \left(\frac{\chi \kappa}{\eta} F_a + 1 \right)^{\frac{2\pi\lambda\gamma}{\chi}} + \left(\frac{\chi \kappa}{\eta} F_a + 1 \right)^{\frac{-1}{2\chi\pi\alpha_2}}. \quad (6)$$

Then, we summarize two regimes for the slow-fronts class (R_3): (1) when χ is high: $E_{system}^{R_3} \rightarrow const.$ and (2) when χ is small or F_a is high: $E_{system}^{R_3} \tilde{\propto} \left(\frac{\chi \kappa}{\eta} F_a \right)^{\frac{2\pi\lambda\gamma}{\chi}}$. It is noteworthy that in the presented results, χ is treated as the order parameter.

In the second part of this section, we use an approach suggested for the left-hand asymmetric shape of the (average) of avalanches in crackling noise systems. Based on this approach [34-25], the asymmetric average shape of the avalanches is due to the role of energy dissipation phenomena (eddy currents and strengthening threshold). Here, we use an equal version for the energy dissipation phenomenon in frictional interfaces, originally proposed in [7,15] to explain the abnormal drop of the phase III (Fig.1a). The interpretation is as follows: a fast-short time fracturing (phase I) induces a very fast increasing the temperature of a tiny ‘‘process zone’’ which cools down in a typical time characteristics (i.e., hardening). The main component of the theory is that the whole of the fracture energy is transferred in to the heat in the process zone (Fig.7). The increased temperature with respect to a reference temperature (room temperature) is as follows:

$$\Delta T = \frac{-\Gamma}{4\rho c_p h} \left[\operatorname{erf}\left(\frac{-h}{\sqrt{4D_T t}}\right) - \operatorname{erf}\left(\frac{h}{\sqrt{4D_T t}}\right) \right] \quad (7)$$

in which $\operatorname{erf}(x) = \frac{2}{\sqrt{\pi}} \sum_{n=0}^{\infty} \frac{x}{2n+1} \prod_{k=1}^n \frac{-x^2}{k} \approx \frac{2}{\sqrt{\pi}} \left(x - \frac{x^3}{3} + \frac{x^5}{10} - \dots \right)$, h is the thickness of the process zone in which the energy rapidly dissipates, D_T is the thermal diffusivity, Γ is the energy released in phase I (or fracture energy), t is the cooling time. With first-order approximation, we estimate t as follows:

$$t \approx \frac{\Gamma^2}{\Theta}, \Theta = 4(\Delta T \rho c_p)^2 \pi D_T \quad (8)$$

in which Θ is a constant value for a given material. From the previous section, we assume $t \approx t_{II}$. Since $RQ_{II} \propto \frac{1}{t_{II}}$ we then discover: $RQ_{II} \propto \frac{\Theta}{\Gamma^2} \Rightarrow E_{pulse}^{II} \propto \Gamma^{-4}$. Then the E_{pulse}^{II} indirectly includes the fracture energy. The implication of the obtained relation is remarkable when we analyse the fracture energy variation while considering the “rupture” velocity-regimes: $E_{pulse}^{II} \propto \overline{\langle T \rangle}^{-1/2, \chi \pi \alpha_2}$ yielding $\Gamma \propto \overline{\langle T \rangle}^{1/8, \chi \pi \alpha_2}$. Considering $\chi < 0$ indicates that decreasing $\overline{\langle T \rangle}$ results in the increment of the rupture velocity (i.e., $\overline{\langle T \rangle} \propto \Xi^\chi$ parameter space), inducing increment of Γ .

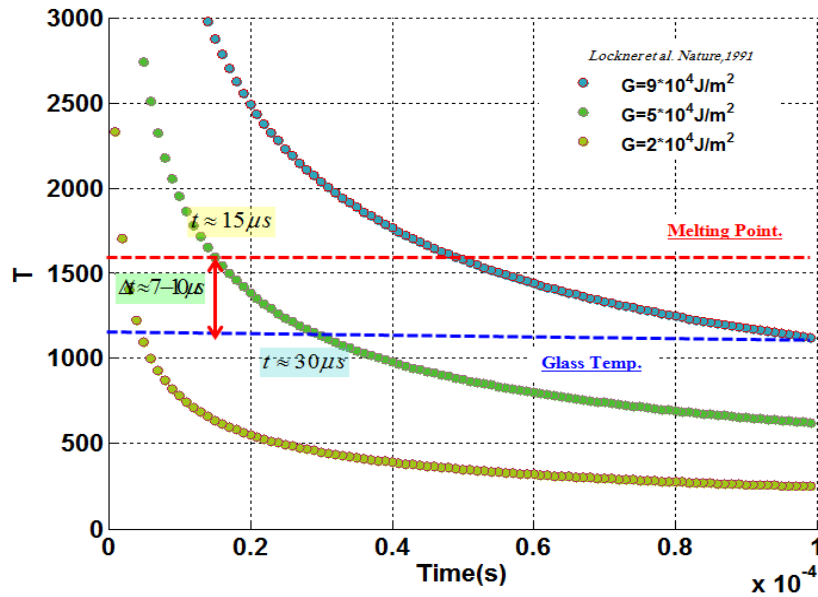


Figure 7|Transition to “rubber-like” phase using 1D heat-diffusion model for a sub-micron process zone. For $G \approx 5 \times 10^4 \text{ Jm}^{-2}$ [], the duration of the second phase $t \approx 30 \mu\text{s}$ is satisfied.

The obtained result is comparable with the results of several investigations regarding the weak increase of Γ with rupture velocity [40-41]. We also can extend the concept of the rate of energy dissipation in a “slow class” regime (R3). In other words, how does fracture energy change in slow-slip regime? In this case $\chi > 0$ and then decreasing $\overline{\langle T \rangle}$ yields decreasing Γ . In other words, far from the cross-over point (from the R3 to the R2 class) and in the slow rupture class, the rate of energy dissipation is low. The latter conclusion has been proved numerically in [42] and recently in [43] through spring-block models. In Fig.7, we have shown how the temperature of the process zone in sub-micron length scale can rise to above melting temperature and glass-point of SiO_2 . The employed fracture energy remarkably does agree with the values reported in [44]. Remarkably, the duration of melting and glass-transition phase are $\sim 15 \mu\text{s}$ and $\sim 10 \mu\text{s}$, respectively. A

possible implication of two-time scales is observation of two stages of evolutions in the second phase: a very fast and fast slip phase leading to break the linearity in the second phase. We will discuss this issue more extensively in a later publication.

Mean-field modeling of friction-networks - we consider a mean-field modeling approach and use the power-law nature of the load distribution (or centrality-Fig.8). To this aim, with the aid of the Barabasi-Albert model (B-A model) [45-46], we assume a nearly constant exponent of the centrality distribution: $P(BC) \sim BC^{-\Omega}, \Omega=3$. As the simplest algorithm to get such distribution, the distribution can be interpreted as $\frac{\partial B.C_i}{\partial t} \propto \frac{B.C_i}{\sum_j B.C_j}$. With this interpretation, we assumed networks' evolution is such that at each time step

the nodes with highest centrality (i.e., load), preferentially, grow in terms of holding more "loads".

We now use some of the introduced scaling relations to simplify the relation. The first scaling law relates centrality to the clustering coefficient (Fig.8c: $\langle B.C \rangle_x \propto \langle C \rangle_x^{-\xi}$) and the second rule connects clustering coefficient to node's degree, where $T_T(k) \propto k^\beta$ [28-29] (T_T is the number of triangles and k is the node's degree). To get the latter relation, we use $T(k) = \binom{k}{2} C_k$ and $\binom{k}{2} \sim \frac{k^2}{2}$, then we find $T_T(k) \propto k^\beta$ and eventually it results in:

$B.C \propto 2k^{\xi(2-\beta)}$. Then, we get:

$$\frac{\partial k_i}{\partial t} \propto \frac{2^\xi}{A} \frac{k_i}{\sum_j k_j^A} \quad (9)$$

in which $A = \xi(2 - \beta)$. Assuming $A=1$ leads to classic scale-free networks. Continuing [47] to approximate a nonlinear growth of the kernel (i.e., $\sum_j k_j^A$), Eq. 9 reads as an exponential approximation of the links' evolu-

tion: $k_i(t) \sim \exp\left(\frac{-2^\xi}{A(A+1)} t^{-A+1}\right)$. Let us assume the distribution of edges follows a power law as well as

$P(k) \propto k^{-\delta}$, in which $\delta = 1 - \xi\beta + 2\xi^2(\Omega - 2)(2 - \beta)$ is obtained by using equalizing expectation values of centrality and node's degree. For $\delta > 0$ (as a classic scale-free networks) and $\xi\beta > 1$, we find $\beta < 2$. Below we will see this finding is comparable with numerical implementation of Eq.9. This numerical proof rationalizes the interpretation of centrality distribution.

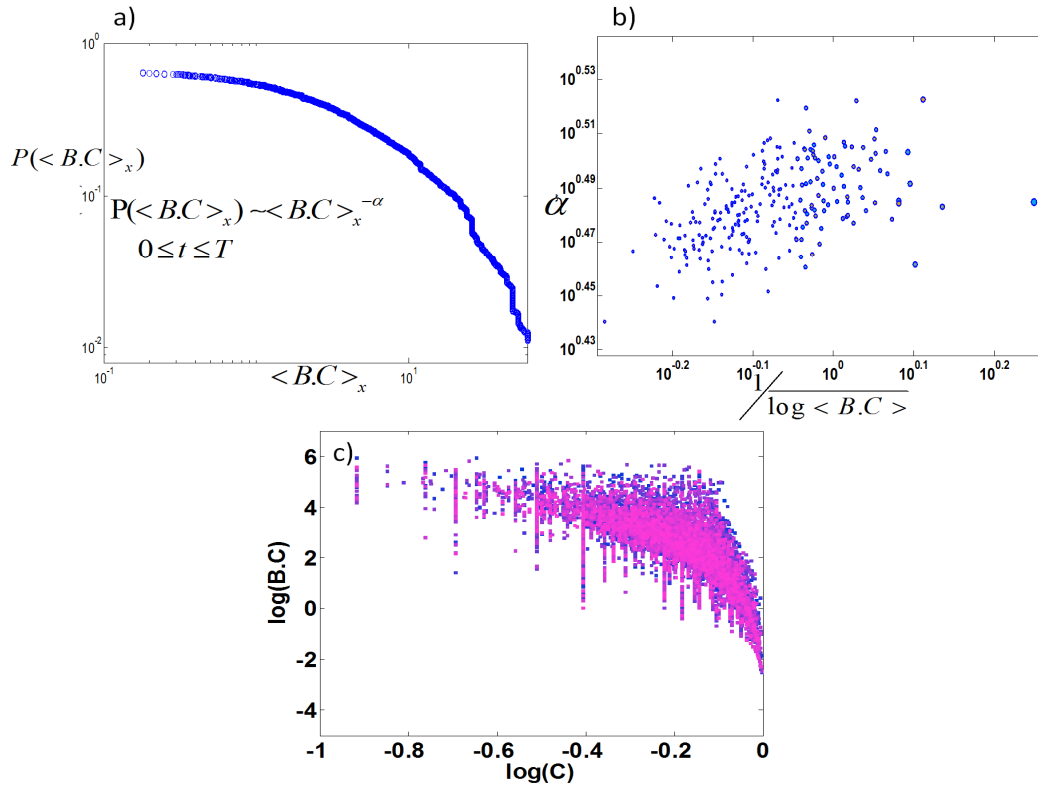


Figure 8| Distribution of centrality. a) Distribution of $\langle B.C \rangle_x$ during the duration of a precursor event ($T=204 \mu s$). **b)** The spatio-temporal average of a few hundreds of Lab.Eq.2 versus the power law coefficient shows that rupture fronts with higher $1/\log \langle B.C \rangle$ holds higher power law coefficient. **c)** The distribution of the sampled points from an events in a log-log scale of $\langle B.C \rangle_x - \langle C \rangle_x$.

We numerically simulate Eq.9 while for each time step we introduce 2 links ($m=2$). After a sufficiently long time evolution, we evaluate the maximum node's degree in the networks while the exponent of the kernel changes (i.e., A)-Fig.9a. A continuous phase transition is observed with increasing A where a systematic transition to “hubness” characteristic ($A \rightarrow 1$) is imprinted in the positive values of the exponent (i.e., $\beta < 2$). This is equal to considering a fast decay of the local information distribution versus the clustering coefficient in which we expect –generally-to evaluate the state of the interface at the first phase (deformation and crushing asperities-Fig.1a). With the increase of the kernel's exponent, the rich nodes do have the chance to grow and naturally the poor nodes (or weak nodes) gradually become suppressed. This is the situation of “the fit - get -rich” (FGR [48])-Fig.9b.

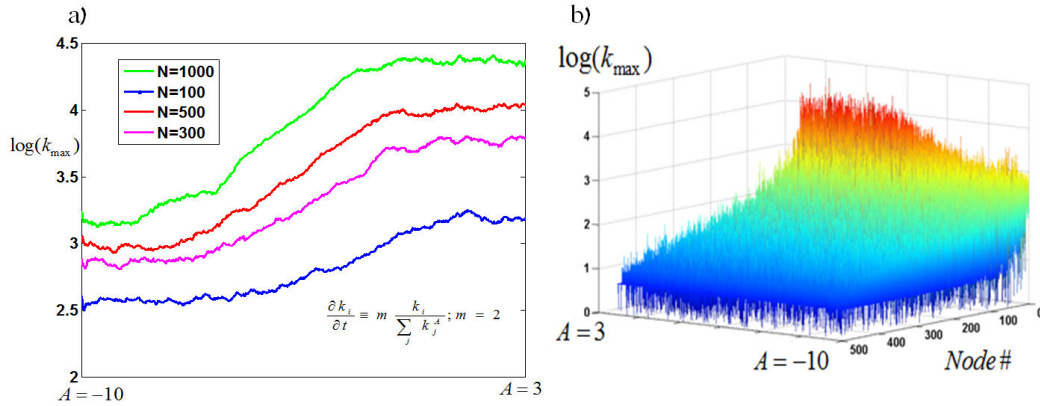


Figure 9(a) The numerical simulation of Eq.9 (see the main text) shows a continuous phase transition (to FGR phase) of links for $t=100,300,500$ and 1000 . (b) The distribution of the node's degree ($t=500$) and evolution of networks to the FGR phase.

Considering the similarity of the Eq.(9) to the fitness model (and non-linear network models [47]), one can examine the possible condensation of the phase transition (or “gel-like” transition) in the present model. One of the possible scenarios is to consider a coupling term in the governing equation with the node's degree evolution. Assuming a non-linear network model [47], we prove if the node's degree is proportional to the ξ and $A \rightarrow 2$, we reach a gel-like state. To maintain the gel-like state, we should satisfy the following condition:

$$\frac{\partial k_i}{\partial t} \equiv \frac{k_i^A}{\sum_j k_j^A}, A \geq 2. \quad \text{Equalizing this condition with the Eq.9 and } A = 2, \text{ we}$$

reach $k_i \propto 2^{\xi-1} \rightarrow k_i \propto \exp(\xi-1) \rightarrow k_i \propto \exp(\frac{2}{2-\beta})$. In other words, around $A = 2$, if the exponent of clustering-

centrality space grows logarithmically proportional with the node's degree. In particular, this situation possibly can be probed in the tail of the distribution in which for $A > 1$, we get: $\langle \xi \rangle \propto \log A + (A-1) \log \langle k \rangle$ where we considered an average value for node's degree and the exponent. Indeed the FGR state corresponds to the R2 or R1 class. Also, we note the rapid decrease of β (or χ) accelerates the growth of k_{\max} , coinciding with the tail of the parameter space in Fig.8a. To present a possible mechanical-interpretation of the condensed state of friction networks, we notice reaching a possible condensed state is equal to approaching a less-collective motion of atoms (i.e., rupture). In particular, the interface does not show collective local stick-slip motion, and the state of the motion of atoms (i.e., particles or nodes) is controlled by a “single” atom or a very condensed of modules of atoms. This phenomenon is the condition of incommensurate contacts; they can prevent collective atomic motion (or collective particle motion), leading to “superlubricity” (or super-rupture) state of the friction [49-50].

Conclusions. –In this work, we presented some novel results regarding a recent proposed approach on functional friction networks. The results showed that the collapsed rupture fronts imprint critical scaling exponents in the proper scalar parameter spaces, comparable with the possible slow and regular deformation or “earthquakes”. Then, we concluded that nearly all recorded events before the main global shear-rupture do flow in a universal critical-line in network parameter spaces. Further analysis of the renormalization group will complete the presented parameter spaces. To further our interpretation of the functional networks, we introduced two different scenarios for the modeling: the first model we analysis the energy of networks based on the change of modularity’s index , helping to infer a possible relationship between the remote stress field as the driving field and the temporal average modularity comparable with the quantified-experimental results. Under the same category and with the aid of the recent fast velocity shear experiments, we modeled each individual event in the proper network spaces, presenting a universal function on sub-micron accelerating/de accelerating damages in brittle materials. Also, Our results showed a singularity in the transition from slow ruptures to sub-Rayleigh class(or vise versa), compatible with the recent direct observation of rupture’s cross-aver in glassy materials. The second model used a mean-filed approximation of networks’ evolution with well-established scale free networks to simulate the evolution of a node’s degree while the governing equation was the result of the collective distribution of events in different network parameter spaces. The model described a transition period to scale-free or fat get rich phase, depending on the variation of the two variables of the model. We also –for the first time -discussed approaching the gel-like (or super-rupture phase) state or mapping the condensation of networks to the super-lubricity state of friction. Obviously, the latter finding need more investigation regarding recorded waveforms in supers hear or super-Rayleigh cases. Collectively, our results showed network theory has a great potential to extract analysis and furthermore model the mechanical phenomena in macroscopic and sub-micron scales. The interpretation of networks parameters in light of nearly constant evolutionary phases might be a great indicator of the evolution of rupture tips and the hidden world around or in vicinity of the rupture tip. In addition to frictional interface, the potential of events originated from different condition such as complex boundary conditions, fluid-driven fractures, noise coupled phenomena such thermal –mechanical cracks, events from high temperature-high pressure (multi-anvil test) and crackling noised from sheared granular materials are our current projects which shall present the mechanism of tiny events and shape of crackling noises in different conditions. Obviously, in this research we used a simplest algorithm to build of networks and we will use weighted networks as well as directed graph theory to get some more insights from macroscopic to micrometer fractures.

Acknowledgements

We would like to acknowledge and thank Dr. D. Lockner (USGS, Menlo-Park, USA) and Stefan Nielsen (Istituto Nazionale di Geofisica e Vulcanologia, Italy) for providing the data set employed in this work.

References

- [1] Meng, L., Inbal, A. & Ampuero, J.-P. A window into the complexity of the dynamic rupture of the 2011 Mw 9 Tohoku-Oki earthquake. *Geophys. Res. Lett.* 38, L00G07 (2011).
- [2] Maercklin, Nils, et al. "Twin ruptures grew to build up the giant 2011 Tohoku, Japan, earthquake." *Scientific reports* 2 (2012).
- [3] Simons, M. et al. The 2011 magnitude 9.0 Tohoku-Oki earthquake: mosaicking the megathrust from seconds to centuries. *Science* 332, 1421–1425 (2011)
- [4] Rubinstein, S., Cohen, G. & Fineberg, J. Detachment fronts and the onset of dynamic friction. *Nature*. 430, 1005-1009 (2004);
- [5] Ben-David, O. Cohen, G. & Fineberg, J. The dynamics of the onset of frictional slip. *Science*. 330, 211 (2010).
- [6] Ben-David, O. Rubinstein, S. & Fineberg, J. Slip-Stick: The evolution of frictional strength. *Nature*. 463, 76 (2010);
- [7] Ghaffari, H. O. & Young, R. P. Acoustic-friction networks and the evolution of precursor rupture fronts in laboratory earthquakes, *Nature Scientific Reports* 3, 1799, doi:10.1038/srep01799.
- [8] Nielsen, S., Taddeucci, J. & Vinciguerra, S. Experimental observation of stick-slip instability fronts. *Geophys. J. Int.* 180, 697 (2010).
- [9] Andrews, D. J. Rupture velocity of plane strain shear cracks. *J. Geophys. Res.* B 81, 5679–5687 (1976).
- [10] Dunham, E.M., Conditions governing the occurrence of supershear ruptures under slip-weakening friction. *J. geophys. Res.* 112, B07302 (2007).
- [11] Rice, J. R., Lapusta, N. & Ranjith, K. Rate and state dependent friction and the stability of sliding between elastically deformable solids. *J. Mech. Phys. Solids* 49, 1865–1898 (2001).
- [12] Noda, Hiroyuki, and Nadia Lapusta. "Stable creeping fault segments can become destructive as a result of dynamic weakening." *Nature* 493.7433 (2013): 518-521.
- [13] Segall, P., Rubin, A. M., Bradley, A. M. & Rice, J. R. Dilatant strengthening as a mechanism for slow slip events. *J. Geophys. Res.* 115, B12305 (2010)
- [14] Shibazaki, B. et al. 3D modeling of the cycle of a great Tohoku-Oki earthquake, considering frictional behavior at low to high slip velocities. *Geophys. Res. Lett.* 38, L21305 (2011).
- [15] Ben-David, O., G. Cohen, and J. Fineberg. "Short-time dynamics of frictional strength in dry friction." *Tribology Letters* 39.3 (2010): 235-245.
- [16] Thompson, B.D., Young, R.P. & Lockner, D.A. Observations of premonitory acoustic emission and slip nucleation during a stick slip experiment in smooth faulted Westerly granite. *Geophys. Res. Lett.* 32 L10304 (2005).
- [17] Thompson, B.D., Young, R.P. & Lockner, D.A. Premonitory acoustic emissions and stick-slip in natural and smooth-faulted Westerly granite. *J. Geophys. Res.* 114, B02205J (2009).
- [18] Marwan, N., Donges, J. F., Zou, Y., Donner, R. V., & Kurths, J. Complex network approach for recurrence analysis of time series. *Physics Letters A*. 373(46), 4246-4254(2009).
- [19] Donner, R. V., Zou, Y., Donges, J. F., Marwan, N., & Kurths, J. Recurrence networks—A novel paradigm for nonlinear time series analysis. *New Journal of Physics*, 12(3), 033025(2010).
- [20] Donner, Reik V., et al. "The geometry of chaotic dynamics—a complex network perspective." *The European Physical Journal B* 84.4 (2011): 653-672.
- [21] Zhang, J., & Small, M. Complex network from pseudoperiodic time series: topology versus dynamics. *Phys. Rev. Lett.* 96(23), 238701(2006).
- [22] Lacasa, L., Luque, B., Ballesteros, F., Luque, J., & Nuño, J. C. From time series to complex networks: the visibility graph. *PNAS*. 105(13), 4972-4975(2008).
- [23] Campanharo, A. S., Simer, M. I., Malmgren, R. D., Ramos, F. M., & Amaral, L. A. N. Duality between time series and networks. *PloS one*. 6(8), e23378(2011).

- [24] Donner, Reik V., et al. "Recurrence-based time series analysis by means of complex network methods." *International Journal of Bifurcation and Chaos* 21.04 (2011): 1019-1046.
- [25] Bassett, D. S., Meyer-Lindenberg, A., Achard, S., Duke, T., & Bullmore, E Adaptive reconfiguration of fractal small-world human brain functional networks. *PNAS*, 103(51), 19518-19523. (2006).
- [26] Donges, Jonathan F., et al. "The backbone of the climate network." *EPL (Europhysics Letters)* 87.4 (2009): 48007.
- [27] Iwayama, K., Hirata, Y., Takahashi, K., Watanabe, K., Aihara, K. & Suzuki, H. Characterizing global evolutions of complex systems via intermediate network representations. *Scientific Reports* 2, 423, (2012).
- [28] Ghaffari, H. O. & Young, R. P. Network configurations of dynamic friction patterns. *EPL* 98 (4), 48003 (2012).
- [29] Ghaffari, H. O. & Young, R. P. Topological complexity of frictional interfaces: friction networks. *Nonlinear Processes Geophys.* 19, 215(2012).
- [30] Newman, M. E. J. & Girvan, M. Finding and evaluating community structure in networks. *Phys. Rev. E* 69, no. 026113 (2004).
- [31] Fortunato, S. Community detection in graphs. *Phys. Rep.* 486, 75–174 (2010).
- [32] Guimerà, R., & Amaral, L. A. N. Functional cartography of complex metabolic networks. *Nature*. 433, 895–900 (2005).
- [33] Newman, M.E.J. *Networks: An Introduction* (Oxford University Press, 2010).
- [34] Mehta, A. P., Mills, A. C., Dahmen, K. A., & Sethna, J. P. Universal pulse shape scaling function and exponents: Critical test for avalanche models applied to Barkhausen noise. *Physical Review E*. 65(4), 046139 (2002).
- [35] Zapperi, S., Castellano, C., Colaiori, F. & Durin, G. Signature of effective mass in crackling-noise asymmetry. *Nature Phys.* 1, 46–49 (2005).
- [36] Sone, Hiroki, and Toshihiko Shimamoto. "Frictional resistance of faults during accelerating and decelerating earthquake slip." *Nature Geoscience* 2.10 (2009): 705-708.
- [37] Xu, X., Zhang, J., & Small, M. Superfamily phenomena and motifs of networks induced from time series. *PNAS*. 105(50), 19601-19605(2008).
- [38] Milo, Ron, et al. "Network motifs: simple building blocks of complex networks." *Science* 298.5594 (2002): 824-827.
- [39] Kashtan, Nadav, and Uri Alon. "Spontaneous evolution of modularity and network motifs." *Proceedings of the National Academy of Sciences of the United States of America* 102.39 (2005): 13773-13778.
- [40] Freund, L. B. The mechanics of dynamic shear crack propagation. *J. Geophys. Res.* 84, 2199–2209 (1979).
- [41] Livne, A., Bouchbinder, E., and Fineberg, J., The breakdown of linear elastic fracture mechanics near the tip of a rapid crack. *Phys. Rev. Lett.* 101, 264301 (2008).
- [42] Braun, O. M., Barel, I. & Urbakh, M. Dynamics of transition from static to kinetic friction. *Phys. Rev. Lett.*, 103, (2009).
- [43] Bouchbinder, E. Brener, E. A., Barel, I. & Urbakh, M. Dynamics at the onset of frictional sliding. *Phys. Rev. Lett.* 107, 235501 (2011).
- [44] Lockner, D. A., Byerlee, J. D., Kuksenko, V., Ponomarev, A., & Sidorin, A. (1991). Quasi-static fault growth and shear fracture energy in granite. *Nature*, 350(6313), 39-42.
- [45] Albert, Réka, and Albert-László Barabási. "Statistical mechanics of complex networks." *Reviews of modern physics* 74.1 (2002): 47.
- [46] Barabási, Albert-László, Réka Albert, and Hawoong Jeong. "Mean-field theory for scale-free random networks." *Physica A: Statistical Mechanics and its Applications* 272.1 (1999): 173-187.
- [47] Krapivsky, P. L.; Redner, S.; Leyvraz, F. (2000). "Connectivity of Growing Random Networks." *Phys. Rev. Lett.* 85: 4629–32.
- [48] Bianconi, G.; Barabási, A.-L. (2001). "Bose–Einstein Condensation in Complex Networks." *Phys. Rev. Lett.* 86: 5632–35.
- [49] Shinjo, K., & Hirano, M. (1993). Dynamics of friction: superlubric state. *Surface Science*, 283(1), 473-478.
- [50] Dienwiebel, M., Verhoeven, G. S., Pradeep, N., Frenken, J. W., Heimberg, J. A., & Zandbergen, H. W. (2004). Superlubricity of graphite. *Physical review letters*, 92(12), 126101.